

Photonic Realization of a Generic Type of Graphene Edge States Exhibiting Topological Flat Band

Shiqi Xia¹, Yongsheng Liang¹, Liqin Tang^{1,2}, Daohong Song^{1,2,*}, Jingjun Xu¹, and Zhigang Chen^{1,2,†}
¹The MOE Key Laboratory of Weak-Light Nonlinear Photonics, TEDA Institute of Applied Physics and School of Physics, Nankai University, Tianjin 300457, China

²Collaborative Innovation Center of Extreme Optics, Shanxi University, Taiyuan, Shanxi 030006, China



(Received 19 January 2023; accepted 26 May 2023; published 6 July 2023)

Cutting a honeycomb lattice (HCL) ends up with three types of edges (zigzag, bearded, and armchair), as is well known in the study of graphene edge states. Here, we propose and demonstrate a distinctive twig-shaped edge, thereby observing new edge states using a photonic platform. Our main findings are (i) the twig edge is a generic type of HCL edge complementary to the armchair edge, formed by choosing the right primitive cell rather than simple lattice cutting or Klein edge modification; (ii) the twig edge states form a complete flat band across the Brillouin zone with zero-energy degeneracy, characterized by nontrivial topological winding of the lattice Hamiltonian; (iii) the twig edge states can be elongated or compactly localized at the boundary, manifesting both flat band and topological features. Although realized here in a photonic graphene, such twig edge states should exist in other synthetic HCL structures. Moreover, our results may broaden the understanding of graphene edge states, as well as new avenues for realization of robust edge localization and nontrivial topological phases based on Dirac-like materials.

DOI: [10.1103/PhysRevLett.131.013804](https://doi.org/10.1103/PhysRevLett.131.013804)

Graphene, a carbon-based monolayer material, has attracted immense attention due to its fundamental interest and highly exploited applications [1]. Edge-dependent electronic states, for example, have been extensively studied, from the physical properties of graphene nanoribbons [1–4] to possible development of graphene-based spintronic devices [5,6]. Apart from two-dimensional electronic materials, various synthetic honeycomb lattices (HCLs) have been employed as artificial graphene for electrons, atoms, and photons [7], which emulate the behavior of electrons in graphene but avoid the limitation and structure instability of real materials. In particular, photonic graphene, an HCL of evanescently coupled waveguide arrays [8], has been proposed and demonstrated as an ideal platform for investigation of graphene edge states [9,10], implemented in various systems, including coupled polariton micropillars [11,12], microwave resonators [13,14] and evanescently coupled waveguide [8]. Perhaps, the most exemplary success lies in the exploration and demonstration of topological physics [15–19], from photonic Floquet topological insulators [15] and valley Hall topological insulators [20,21], to topological surface-emitting lasers [22–24].

Thus far, three types of edges in graphene have been studied: the zigzag, bearded, and armchair edges [4]. The defect-free armchair edge has no edge state, whereas zigzag and bearded edges have a complementary set of nearly degenerate edge states in the one-dimensional Brillouin zone (1D BZ) [1,4]. Such electronic edge states have been observed at the zigzag edge or structured armchair

edges [25–29]. Although the bearded (Klein) edge states have never been observed in real graphene owing to the mechanical instability of the dangling carbon bond, they were realized in the optical analog of graphene—the photonic graphene [10]. Theoretical analyses have shown that these edge states are topologically characterized by the winding properties of the bulk Hamiltonian [30,31]. In addition, other edge geometries including decorated armchair edges with Klein nodes have also been proposed by edge modification [32,33]. While the topological properties and relations of the three known edges are still an active subject, a natural question arises: is there a fourth type of edge distinct from the three known edges? If there is, what is its unique feature?

In this work, in contradistinction to the widely investigated edges in graphene, we propose and demonstrate a new type of edge, which we shall name “twig edge” due to its shape. We unveil that it is a generic type of edge in HCLs by considering the primitive-cell generator rather than a simple lattice truncation or cutting the bulk along a chosen direction. Our analysis suggests that the twig edge together with three other edge conditions represents the fundamental and complete basis of HCLs, and other decorated or modified edges can be viewed as their combinations. We show that the twig edge enables a set of zero-energy edge states which form a 1D dispersionless flat band complementary to the armchair edge, characterized by the nontrivial winding of the (gauge-dependent) Bloch Hamiltonian. Experimentally, we establish a photonic graphene with the twig edge using a laser-writing technique

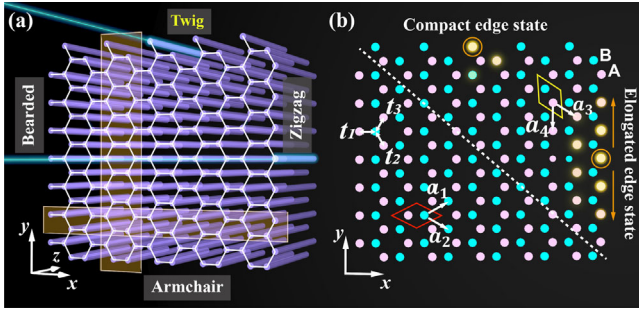


FIG. 1. Illustration of HCLs with four different edge conditions. (a) Schematic of an HCL with four distinct types of edges. Two shaded rectangles illustrate supercells for bearded or zigzag (horizontal) and twig or armchair (vertical) edges. A probe beam aiming at single site of the twig (zigzag) edge will be compact (elongated) along the edge, indicated by bright yellow dots in (b). (b) HCL structure with two sublattices (A, B) in (x, y) plane. The white dashed line is merely used to separate the two parts in the HCL that are described by different unit cells and Bloch Hamiltonian. The unit cell enclosed by a red (yellow) rhombus is for bearded or armchair (zigzag or twig) edges. $\mathbf{a}_1, \mathbf{a}_2$ and $\mathbf{a}_3, \mathbf{a}_4$ are the corresponding basis vectors when different unit cells are selected. $\mathbf{a}_1 = \sqrt{3}a/2\hat{x} + a/2\hat{y}$, $\mathbf{a}_2 = \sqrt{3}a/2\hat{x} - a/2\hat{y}$ and $\mathbf{a}_3 = \sqrt{3}a/2\hat{x} - a/2\hat{y}$, $\mathbf{a}_4 = -a\hat{y}$, a is the lattice constant. Double headed arrows for t_1, t_2, t_3 mark the three nearest couplings from any chosen B site.

and realize, to the best of our knowledge, the first observation of both elongated and highly compact edge states at the twig edge without employing any defect or nonlinearity.

We first discuss the formation of different edges of graphene [Fig. 1(a)] along with their edge state properties. One kind of unit cell for the HCL structure is sketched in the lower left corner of Fig. 1(b) (red rhombus) with two assigned basic vectors ($\mathbf{a}_1, \mathbf{a}_2$). For an infinite lattice (or under a periodic boundary condition), the bulk Bloch Hamiltonian from this chosen unit cell is

$$\mathcal{H}_{BA}(\mathbf{k}) = \begin{bmatrix} 0 & \Delta_{BA}(\mathbf{k}) \\ \Delta_{BA}^*(\mathbf{k}) & 0 \end{bmatrix},$$

$$\Delta_{BA}(\mathbf{k}) = t_1 + t_2 e^{ika_2} + t_3 e^{ika_1}, \quad (1)$$

where t_1 is the intracell coupling and t_2, t_3 are the intercell couplings [Fig. 1(b)], the subscript BA indicates *bearded* edge and *armchair* edge. By translating the unit cell, the HCL with these two edges can be obtained [see the left and bottom edges in Fig. 1(b)]. The band structure along the k_x (k_y) direction is calculated by properly choosing the vertical (horizontal) supercell marked by a shaded rectangle in Fig. 1(a). As has been shown before [4], the bearded edge supports edge states residing between two Dirac points in the 1D BZ, whereas the armchair edge has none. On the other hand, one can also have a different choice of unit cell [yellow rhombus in upper right corner of

Fig. 1(b)], where the basic vectors are changed to $(\mathbf{a}_3, \mathbf{a}_4)$. Translating this unit cell leads to the formation of HCL with zigzag and twig edges [see the right and top edges in Fig. 1(b)]. Similar to Eq. (1), the associated bulk Bloch Hamiltonian $\mathcal{H}_{ZT}(\mathbf{k})$ for the *zigzag* and *twig* edges becomes

$$\mathcal{H}_{ZT}(\mathbf{k}) = \begin{bmatrix} 0 & \Delta_{ZT}(\mathbf{k}) \\ \Delta_{ZT}^*(\mathbf{k}) & 0 \end{bmatrix},$$

$$\Delta_{ZT}(\mathbf{k}) = t_1 e^{ika_3} + t_2 + t_3 e^{ika_4}, \quad (2)$$

where t_2 (t_1, t_3) become the intracell (intercell) couplings [Fig. 1(b)]. Note that each unit cell and the corresponding Bloch Hamiltonian describe two distinct edge conditions along x and y directions.

In this work, we focus our analysis on the twig edge and its relations with others. The properties of twig edge are described by \mathcal{H}_{ZT} along the x direction (top-right part in Fig. 1). The zigzag edge states are denoted by the red lines in momentum space [Fig. 2(a1)], with a spectrum region complementary to that of the bearded edge states [4,10]. For the twig edge, as shown in Fig. 2(a2), it supports a unique topological flat band constructed by the edge states across the entire 1D BZ. The energy of twig edge states is only distributed at the B sublattices on the top boundary and exponentially decays into the bulk [Fig. 2(c)]. Such zero-energy edge states in graphene are attributed to the bulk topological properties and can be analytically derived from the ‘‘bulk-boundary correspondence’’ [31,34]. For the HCL with chiral symmetry, the topological invariant can be described by the winding number [30]

$$w = \frac{1}{2\pi} \oint \frac{d}{dk} \arg[\Delta(\mathbf{k})] dk, \quad (3)$$

where \mathbf{k} can be k_x or k_y component depending on the edge direction, and $\Delta(\mathbf{k})$ is the off-diagonal term of bulk Hamiltonian. Considering the zigzag and twig edges, the bulk Hamiltonian can be rewritten as $\mathcal{H}_{ZT}(\mathbf{k}) = \mathbf{h}_{ZT}(\mathbf{k}) \cdot \boldsymbol{\sigma}$, where $\mathbf{h}_{ZT}(\mathbf{k}) = \{\text{Re}[\Delta_{ZT}(\mathbf{k})], \text{Im}[\Delta_{ZT}(\mathbf{k})]\}$, and the Pauli matrix $\boldsymbol{\sigma} = (\sigma_x, \sigma_y)$. To calculate the winding number for the zigzag edge, the Bloch vector k_y is fixed and the orientation of $\mathbf{h}_{ZT}(\mathbf{k})$ varies along k_x , as illustrated by the blue arrows in Fig. 2(b). If $\mathbf{h}_{ZT}(\mathbf{k})$ rotates to make a whole loop within a period of k_x , w is nonzero which leads to the presence of edge states at the given k_y . The shaded regions in Fig. 2(b) demonstrate the values of k_y for which nontrivial winding leads to the zigzag edge states, consistent with the results in Fig. 2(a1). To directly illustrate their winding path, $\mathbf{h}_{ZT}(\mathbf{k})$ with different k_y is plotted in the (σ_x, σ_y) plane in Fig. 2(d). The origin point \mathcal{O} marked by a red dot in Figs. 2(d2) and 2(e1) is the gap closing and phase transition point [35]. When \mathcal{O} is encircled by the winding loop [Fig. 2(d3)], it falls in the shaded region in Fig. 2(b) where the edge states exist

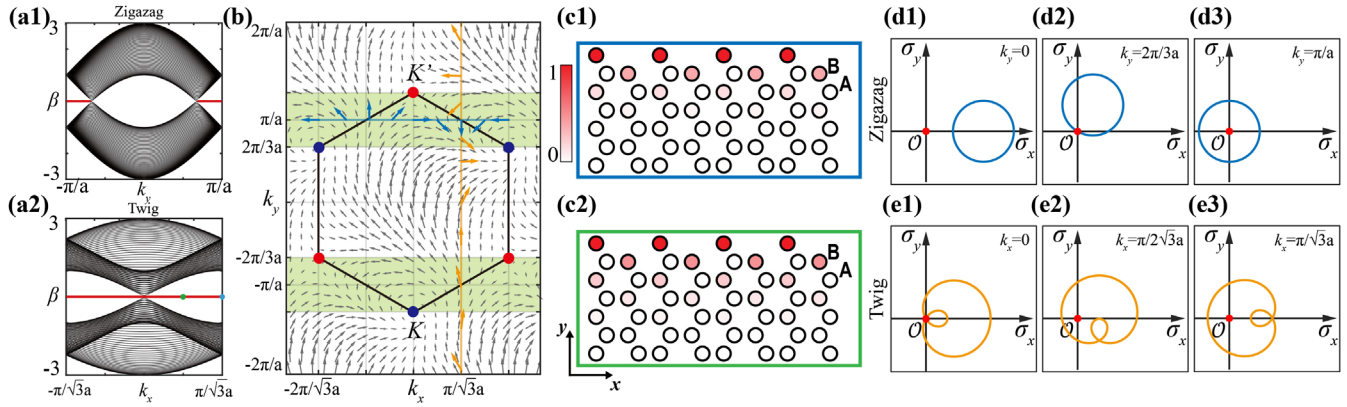


FIG. 2. Theoretical analysis of the topological property of zigzag or twig edge states in HCLs. (a) 1D band structures for HCL with (a1) zigzag and (a2) twig edges, where the red lines represent the regions of edge states. (b) Vector fields of $\mathbf{h}_{ZT}(\mathbf{k})$. Red and blue dots represent two inequivalent Dirac points K and K' at corners of the first BZ. The values of k_y at the shaded regions indicate the zigzag edge with nontrivial winding, where blue arrows indicate the direction of the vector field along $k_y = \pi/a$. Twig edge states exist for any k_x , and orange arrows are for that of the twig edge at $k_x = \pi/\sqrt{3}a$. (c) Normalized intensity distributions of twig edge states at (c1) $k_x = \pi/\sqrt{3}a$ and (c2) $k_x = \pi/2\sqrt{3}a$ denoted by blue and green dots in (a2), respectively. (d) Winding loops for the zigzag edge in the (σ_x, σ_y) plane at different k_y . The red dot marks the origin \mathcal{O} . (e) has the same layout as (d) but for the twig edge at different k_x .

with a nonzero winding number. The other two loops in Figs. 2(d1) and 2(d2) correspond to the trivial and transitional cases at $k_y = 0$ and $k_y = 2\pi/3a$. On the other hand, when $\mathbf{h}_{ZT}(\mathbf{k})$ is employed to analyze the topological properties for the twig edge, k_y varies constantly for any k_x , and an example at $k_x = \pi/\sqrt{3}a$ is shown by the vertical line in Fig. 2(b). The winding loops always encircle \mathcal{O} in the (σ_x, σ_y) plane, except at the gap closing point at $k_x = 0$ [Fig. 2(e)]. As such, the twig edge states exist and are characterized by *nontrivial* winding throughout the whole 1D BZ, forming a topological flat band. Such a complete flat band found at the twig edge differs from the “assembled” flat band consisting of edge states supported by different (zigzag-bearded) HCL edges [4]. Moreover, in contrast to the unconventional edge states found at the bearded edge in photonic graphene [10], we did not find any additional edge state at the twig edge even with a continuous model.

We emphasize our approach for understanding the relation between bulk topological properties and edge conditions in graphene: to unveil the topological nature of edge states, the edges should be considered from “piling up” the unit cells instead of specific truncations of the HCL. Thus, the boundary sites must be contained within a complete unit cell. For instance, by comparing \mathcal{H}_{BA} and \mathcal{H}_{ZT} , one can see $\Delta_{ZT}(\mathbf{k}) = \exp(ika_3)\Delta_{BA}(\mathbf{k})$ due to the different orientations of basic vectors. When only the bulk property of the system is considered, the gauge term in different bulk Hamiltonians has no physical effect. However, once the edges are considered, one unique bulk Hamiltonian is selected, and the topological features along k_x and k_y are affected by the gauge term [Eq. (3)], which in turn determines the existence of edge states. Such gauge dependence of edge states does not conflict with the gauge

invariant of the Berry phase derived from a given bulk Hamiltonian; rather, it reflects that the gauge-field effect can be “physical,” as manifested from the nontrivial topological states at different edges. The interplays between the edge conditions and the winding properties of bulk Hamiltonian reveal the distinctive feature of zero-energy edge states.

Next, we present experimental realization of twig edge states using photonic graphene, along with numerical simulations. The photonic HCL with the desired edge structure is established by the cw-laser writing technique in a nonlinear crystal (SBN) [37]. Such an HCL with two twig (top and bottom) and zigzag (left and right) edges is shown in Fig. 3(a), with a lattice spacing of $32 \mu\text{m}$. To excite the twig edge states, a probe beam with specific amplitude and phase distribution matching that of the theoretically calculated edge mode [Fig. 2(c)] is launched into the HCL at the top edge [35]. To show that the twig edge states exist in a large momentum region, the probe beam with two different transverse momenta is selected, matching the blue-point (green-point) excitation at $k_x = \pi/\sqrt{3}a$ ($k_x = \pi/2\sqrt{3}a$) in Fig. 2(a2). Notably, the zigzag or the bearded edge cannot support edge states simultaneously at these two relative spectral positions in the 1D BZ. At the twig edge, however, the probe beam remains localized at the edge and populates only the B sublattices after 20 mm of propagation through the lattice [Figs. 3(b1) and 3(b2)], forming the edge states in agreement with calculated results [Figs. 2(c1) and 2(c2)]. The leakage of energy to the A sites at the two ends (outside of the dashed square) is mainly due to the finite-size effects along the x direction. For comparison, the mixed bulk modes are excited at $k = 0$ when the probe is sent to the edge [35]. The output of the probe beam with mixed bulk modes

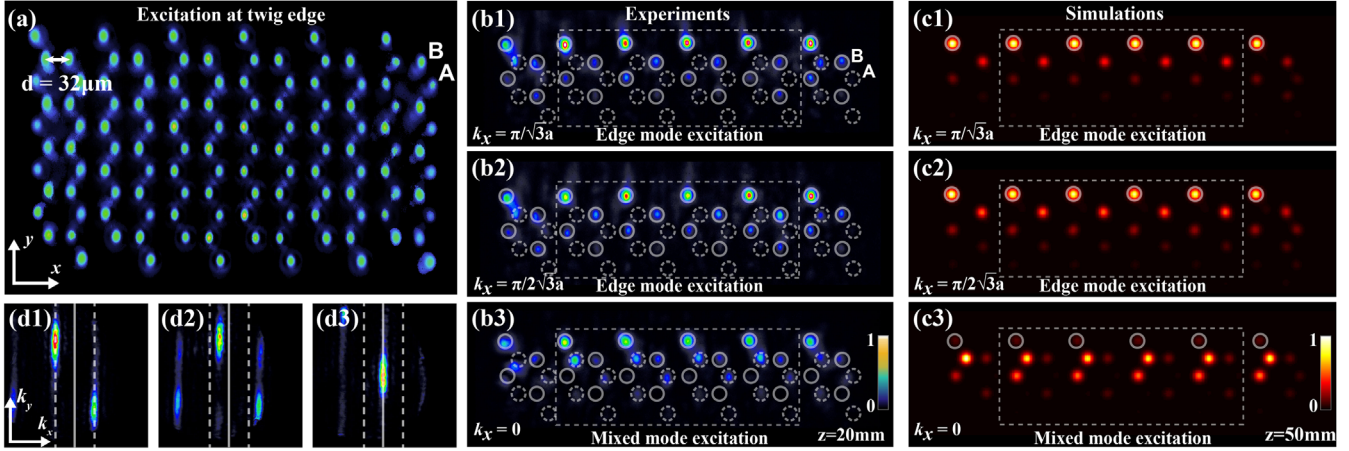


FIG. 3. Experimental and numerical demonstration of the twig edge states in photonic graphene. (a) An HCL with twig edges along the x direction established in the experiment. $d = 32 \mu\text{m}$ is the distance between nearest sites. (b1),(b2) Experimental outputs of the probe beams which match the eigenmode of twig edge states at (b1) $k_x = \pi/\sqrt{3}a$ and (b2) $k_x = \pi/2\sqrt{3}a$. (b3) The output for the mixed mode excitation at $k_x = 0$. The corresponding simulation results for a longer propagation distance ($z = 50 \text{ mm}$) are shown in (c), where the solid white circles mark the topmost sites of the twig edge. (d) Fourier spectra of the input beams corresponding to (b), in which solid (dashed) lines mark the center (edge) of the 1D BZ.

cannot be localized on the edge and couples into the A sublattice [Fig. 3(b3)], which contrasts with that in Figs. 3(b1)–3(b2). To explicitly show the excitation condition, the Fourier spectra of the probe beam are experimentally captured and shown in Fig. 3(d), corresponding to the edge and middle spectral components of the 1D BZ. Since the propagation distance in experiment is limited by the crystal length, numerical simulations to a long propagation distance are presented in Fig. 3(c) to better differentiate the dynamics: for the edge mode excitation, light remains edge localized although the mode profile changes slightly at longer propagation distances; but for the mixed mode excitation, it spreads into the bulk occupying both A and B sublattice sites, resulting in a pronounced change of

the profile. More experimental results can be found in Supplemental Material [35].

Since all twig edge states are degenerate and form a dispersionless flat band, it enables the formation of the compact edge state along the boundary [27,38–41]. We demonstrate the edge excitation at the zigzag and twig edges for comparison, which share the same bulk Hamiltonian but the zigzag edge states occupy only a portion of the 1D BZ. By selecting a site along different edges and removing all the mode components of dispersive bands, the modified edge states are obtained and are shown in Figs. 4(a1) and 4(c1) for twig and zigzag edges. Most of light along twig edge is in one supercell [Fig. 4(a2)], while that of the zigzag edge state elongates to neighbor sites along the edge [Fig. 4(c2)].

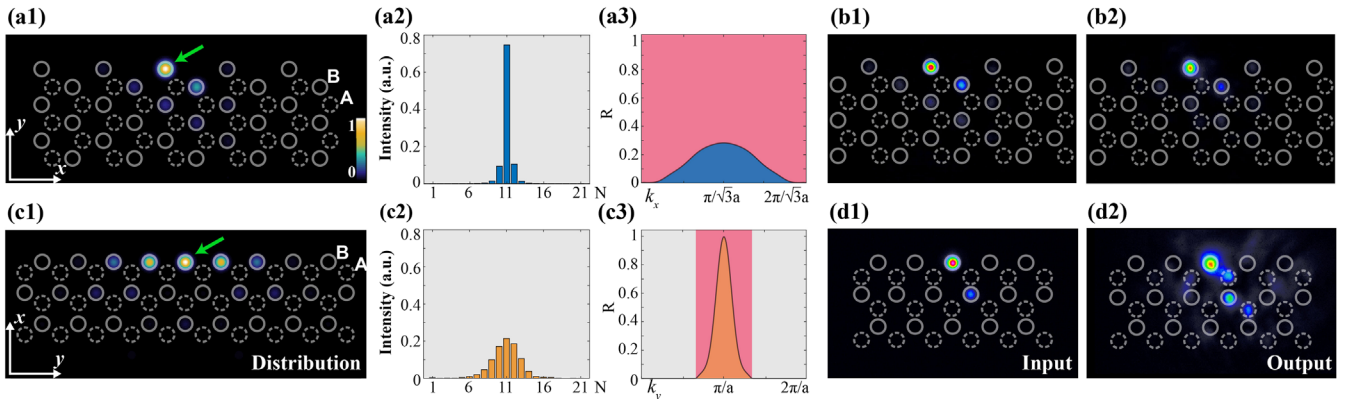


FIG. 4. Demonstration of compact edge states at the twig edge of photonic graphene. (a) Theoretical results of a compact edge state for the twig edge. (a1) The intensity distribution of the modified edge state. The initial selected site is marked by a green arrow. (a2) The percentage of energy projected on supercells (N) along the boundary. (a3) The spectrum distribution of the compact edge state in k space, where edge states exist in the red shaded region. (b) Experimental results of a compact edge state. (b1) A probe beam matching the compact edge state at the input. (b2) The output of the probe beam after 20 mm propagation. (c),(d) have the same layout as (a),(b) but obtained from the zigzag edge for a direct comparison.

The mode mapping $R = |\langle \varphi_k | \Psi \rangle|^2$ is defined to show the distribution of such edge state in momentum space, where Ψ is the modified edge state shown in Figs. 4(a1) and 4(c1) and φ_k denotes the edge eigenstate at momentum k . The modified edge state along the twig edge spans the entire 1D BZ [Fig. 4(a3)], indicating a more compact form along the boundary in real space compared to that at the zigzag edge [Fig. 4(c3)]. We call the edge state shown in Fig. 4(a1) “compact edge state.” To demonstrate such a distinctive compact feature of twig edge states in experiment, the probe beam which matches the compact edge state [Fig. 4(b1)] is sent to the lattice, and it remains intact and compact after 20 mm propagation [Fig. 4(b2)]. On the other hand, when the same probe beam excites only one supercell along the zigzag edge [Fig. 4(d1)], it cannot support the compact edge state, and light spreads into A sublattices [Fig. 4(d2)]. These experimental results illustrate the unique feature of the compact edge state originating from the topological flat band formed by the degenerated edge eigenstates.

In summary, we have demonstrated a new type of graphene edge state using a photonic platform. The new twig edge forms a complete set of edge conditions together with three other well-known edges. We have discussed the topological origin of the edge states, unraveling the relation between edge conditions and the bulk topological properties. Moreover, soliton-like compact edge states exhibiting both flat band and topological features are observed without employing any defect or nonlinearity. Realization of the twig edge and its characteristic edge states in HCLs opens up an avenue for fundamental research in many areas, such as the valley Hall effect and topological corner and edge states [15,21,41–45] in Dirac-like systems, which may lead to subsequent development of unconventional application devices.

We thank H. Buljan for helpful discussion. This work was supported by National Key R&D Program of China (2022YFA1404800), the National Natural Science Foundation of China (No. 12134006, No. 12274242, No. 11922408, No. 12204252), China Postdoctoral Science Foundation (No. BX2021134, No. 2021M701790), and the Natural Science Foundation of Tianjin for Distinguished Young Scholars (No. 21JCJQC00050), Program for Changjiang Scholars and Innovative Research Team in University (IRT_13R29), 111 Project (No. B23045) in China.

X. S. and L. Y. have contributed equally to this work.

* songdaohong@nankai.edu.cn

† zgchen@nankai.edu.cn

[1] A. H. Castro Neto, F. Guinea, N. M. R. Peres, K. S. Novoselov, and A. K. Geim, The electronic properties of graphene, *Rev. Mod. Phys.* **81**, 109 (2009).

- [2] K. Nakada, M. Fujita, G. Dresselhaus, and M. S. Dresselhaus, Edge state in graphene ribbons: Nanometer size effect and edge shape dependence, *Phys. Rev. B* **54**, 17954 (1996).
- [3] L. Brey and H. A. Fertig, Electronic states of graphene nanoribbons studied with the Dirac equation, *Phys. Rev. B* **73**, 235411 (2006).
- [4] M. Kohmoto and Y. Hasegawa, Zero modes and edge states of the honeycomb lattice, *Phys. Rev. B* **76**, 205402 (2007).
- [5] Y.-W. Son, M. L. Cohen, and S. G. Louie, Half-metallic graphene nanoribbons, *Nature (London)* **444**, 347 (2006).
- [6] O. V. Yazyev and M. I. Katsnelson, Magnetic Correlations at Graphene Edges: Basis for Novel Spintronics Devices, *Phys. Rev. Lett.* **100**, 047209 (2008).
- [7] M. Polini, F. Guinea, M. Lewenstein, H. C. Manoharan, and V. Pellegrini, Artificial honeycomb lattices for electrons, atoms and photons, *Nat. Nanotechnol.* **8**, 625 (2013).
- [8] O. Peleg, G. Bartal, B. Freedman, O. Manela, M. Segev, and D. N. Christodoulides, Conical Diffraction and Gap Solitons in Honeycomb Photonic Lattices, *Phys. Rev. Lett.* **98**, 103901 (2007).
- [9] M. C. Rechtsman, Y. Plotnik, J. M. Zeuner, D. Song, Z. Chen, A. Szameit, and M. Segev, Topological Creation and Destruction of Edge States in Photonic Graphene, *Phys. Rev. Lett.* **111**, 103901 (2013).
- [10] Y. Plotnik, M. C. Rechtsman, D. Song, M. Heinrich, J. M. Zeuner, S. Nolte, Y. Lumer, N. Malkova *et al.*, Observation of unconventional edge states in “photonic graphene,” *Nat. Mater.* **13**, 57 (2014).
- [11] M. Milicevic, T. Ozawa, G. Montambaux, I. Carusotto, E. Galopin, A. Lemaitre, L. Le Gratiet, I. Sagnes, J. Bloch, and A. Amo, Orbital Edge States in a Photonic Honeycomb Lattice, *Phys. Rev. Lett.* **118**, 107403 (2017).
- [12] O. Jamadi, E. Rozas, G. Salerno, M. Milićević, T. Ozawa, I. Sagnes, A. Lemaitre, L. Le Gratiet *et al.*, Direct observation of photonic Landau levels and helical edge states in strained honeycomb lattices, *Light Sci. Appl.* **9**, 144 (2020).
- [13] M. Bellec, U. Kuhl, G. Montambaux, and F. Mortessagne, Manipulation of edge states in microwave artificial graphene, *New J. Phys.* **16**, 113023 (2014).
- [14] M. Bellec, C. Poli, U. Kuhl, F. Mortessagne, and H. Schomerus, Observation of supersymmetric pseudo-Landau levels in strained microwave graphene, *Light Sci. Appl.* **9**, 146 (2020).
- [15] M. C. Rechtsman, J. M. Zeuner, Y. Plotnik, Y. Lumer, D. Podolsky, F. Dreisow, S. Nolte, M. Segev, and A. Szameit, Photonic Floquet topological insulators, *Nature (London)* **496**, 196 (2013).
- [16] A. B. Khanikaev, S. Hossein Mousavi, W.-K. Tse, M. Kargarian, A. H. MacDonald, and G. Shvets, Photonic topological insulators, *Nat. Mater.* **12**, 233 (2013).
- [17] M. Hafezi, S. Mittal, J. Fan, A. Migdall, and J. M. Taylor, Imaging topological edge states in silicon photonics, *Nat. Photonics* **7**, 1001 (2013).
- [18] L.-H. Wu and X. Hu, Scheme for Achieving a Topological Photonic Crystal by Using Dielectric Material, *Phys. Rev. Lett.* **114**, 223901 (2015).
- [19] T. Ozawa, H. M. Price, A. Amo, N. Goldman, M. Hafezi, L. Lu, M. C. Rechtsman, D. Schuster *et al.*, Topological photonics, *Rev. Mod. Phys.* **91**, 015006 (2019).

- [20] T. Ma and G. Shvets, All-Si valley-Hall photonic topological insulator, *New J. Phys.* **18**, 025012 (2016).
- [21] J. Noh, S. Huang, K. P. Chen, and M. C. Rechtsman, Observation of Photonic Topological Valley Hall Edge States, *Phys. Rev. Lett.* **120**, 063902 (2018).
- [22] A. Dikopoltsev, T. H. Harder, E. Lustig, O. A. Egorov, J. Beierlein, A. Wolf, Y. Lumer, M. Emmerling *et al.*, Topological insulator vertical-cavity laser array, *Science* **373**, 1514 (2021).
- [23] L. Yang, G. Li, X. Gao, and L. Lu, Topological-cavity surface-emitting laser, *Nat. Photonics* **16**, 279 (2022).
- [24] R. Contractor, W. Noh, W. Redjem, W. Qarony, E. Martin, S. Dhuey, A. Schwartzberg, and B. Kanté, Scalable single-mode surface-emitting laser via open-Dirac singularities, *Nature (London)* **608**, 692 (2022).
- [25] Y. Kobayashi, K.-i. Fukui, T. Enoki, K. Kusakabe, and Y. Kaburagi, Observation of zigzag and armchair edges of graphite using scanning tunneling microscopy and spectroscopy, *Phys. Rev. B* **71**, 193406 (2005).
- [26] C. Tao, L. Jiao, O. V. Yazyev, Y.-C. Chen, J. Feng, X. Zhang, R. B. Capaz, J. M. Tour *et al.*, Spatially resolving edge states of chiral graphene nanoribbons, *Nat. Phys.* **7**, 616 (2011).
- [27] P. Ruffieux, S. Wang, B. Yang, C. Sánchez-Sánchez, J. Liu, T. Dienel, L. Talirz, P. Shinde *et al.*, On-surface synthesis of graphene nanoribbons with zigzag edge topology, *Nature (London)* **531**, 489 (2016).
- [28] O. Gröning, S. Wang, X. Yao, C. A. Pignedoli, G. Borin Barin, C. Daniels, A. Cupo, V. Meunier *et al.*, Engineering of robust topological quantum phases in graphene nanoribbons, *Nature (London)* **560**, 209 (2018).
- [29] H. Wang, H. S. Wang, C. Ma, L. Chen, C. Jiang, C. Chen, X. Xie, A.-P. Li, and X. Wang, Graphene nanoribbons for quantum electronics, *Nat. Rev. Phys.* **3**, 791 (2021).
- [30] S. Ryu and Y. Hatsugai, Topological Origin of Zero-Energy Edge States in Particle-Hole Symmetric Systems, *Phys. Rev. Lett.* **89**, 077002 (2002).
- [31] P. Delplace, D. Ullmo, and G. Montambaux, Zak phase and the existence of edge states in graphene, *Phys. Rev. B* **84**, 195452 (2011).
- [32] K. Wakabayashi, S. Okada, R. Tomita, S. Fujimoto, and Y. Natsume, Edge states and flat bands of graphene nanoribbons with edge modification, *J. Phys. Soc. Jpn.* **79**, 034706 (2010).
- [33] W. Jaskólski, A. Ayuela, M. Pelc, H. Santos, and L. Chico, Edge states and flat bands in graphene nanoribbons with arbitrary geometries, *Phys. Rev. B* **83**, 235424 (2011).
- [34] R. S. K. Mong and V. Shivamoggi, Edge states and the bulk-boundary correspondence in Dirac Hamiltonians, *Phys. Rev. B* **83**, 125109 (2011).
- [35] See Supplemental Material at <http://link.aps.org/supplemental/10.1103/PhysRevLett.131.013804> for details of theoretical analysis on topological properties of HCL edge states, experimental methods, and results, which includes Ref. [36].
- [36] T. Kreis, Digital holographic interference-phase measurement using the Fourier-transform method, *J. Opt. Soc. Am. A* **3**, 847 (1986).
- [37] S. Xia, A. Ramachandran, S. Xia, D. Li, X. Liu, L. Tang, Y. Hu, D. Song *et al.*, Unconventional Flatband Line States in Photonic Lieb Lattices, *Phys. Rev. Lett.* **121**, 263902 (2018).
- [38] R. A. Vicencio, C. Cantillano, L. Morales-Inostroza, B. Real, C. Mejía-Cortés, S. Weimann, A. Szameit, and M. I. Molina, Observation of Localized States in Lieb Photonic Lattices, *Phys. Rev. Lett.* **114**, 245503 (2015).
- [39] S. Mukherjee, A. Spracklen, D. Choudhury, N. Goldman, P. Öhberg, E. Andersson, and R. R. Thomson, Observation of a Localized Flat-Band State in a Photonic Lieb Lattice, *Phys. Rev. Lett.* **114**, 245504 (2015).
- [40] D. Leykam, A. Andreanov, and S. Flach, Artificial flat band systems: From lattice models to experiments, *Adv. Phys.* **3**, 1473052 (2018).
- [41] J.-W. Rhim and B.-J. Yang, Classification of flat bands according to the band-crossing singularity of Bloch wave functions, *Phys. Rev. B* **99**, 045107 (2019).
- [42] J. Noh, W. A. Benalcazar, S. Huang, M. J. Collins, K. P. Chen, T. L. Hughes, and M. C. Rechtsman, Topological protection of photonic mid-gap defect modes, *Nat. Photonics* **12**, 408 (2018).
- [43] A. El Hassan, F. K. Kunst, A. Moritz, G. Andler, E. J. Bergholtz, and M. Bourennane, Corner states of light in photonic waveguides, *Nat. Photonics* **13**, 697 (2019).
- [44] H. Xue, Y. Yang, F. Gao, Y. Chong, and B. Zhang, Acoustic higher-order topological insulator on a kagome lattice, *Nat. Mater.* **18**, 108 (2019).
- [45] X. Zhang, L. Liu, M.-H. Lu, and Y.-F. Chen, Valley-Selective Topological Corner States in Sonic Crystals, *Phys. Rev. Lett.* **126**, 156401 (2021).